

# Compositional Embeddings for Multi-Label One-Shot Learning

Zeqian Li<sup>1</sup> Mike Mozer<sup>2</sup> Jacob Whitehill<sup>1</sup>

## Abstract

We explore the idea of *compositional set embeddings* that can be used to infer not just a single class per input (e.g., image, audio signal), but a set of classes, in the setting of one-shot learning. Class compositionality is useful in tasks such as multi-object detection in images and multi-speaker diarization in audio. Specifically, we devise and implement two novel models consisting of (1) an embedding function  $f$  trained jointly with a “composite” function  $g$  that computes *set union* operations between the classes encoded in two embedding vectors; and (2) embedding  $f$  trained jointly with a “query” function  $h$  that computes whether the classes encoded in one embedding *subsume* the classes encoded in another embedding. In contrast to prior work, these models must both *perceive* the classes associated with the input examples and *encode* the relationships between different class label sets. In experiments on the OmniGlot, LibriSpeech and Open Images datasets, the proposed compositional embedding models outperform baselines based on traditional embedding methods.

## 1. Introduction

Embeddings, especially as enabled by advances in deep learning, have found widespread use in natural language processing, object recognition, face identification and verification, speaker verification and diarization (i.e., who is speaking when; Sell et al., 2018), and other areas. What embedding functions have in common is that they map their input into a fixed-length distributed representation (i.e., continuous space) that facilitates more efficient and accurate (Scott et al., 2018) downstream analysis than simplistic representations such as one-of- $k$ . Moreover, they are amenable to one-shot and few-shot learning since the set of classes that can be represented does not depend directly on

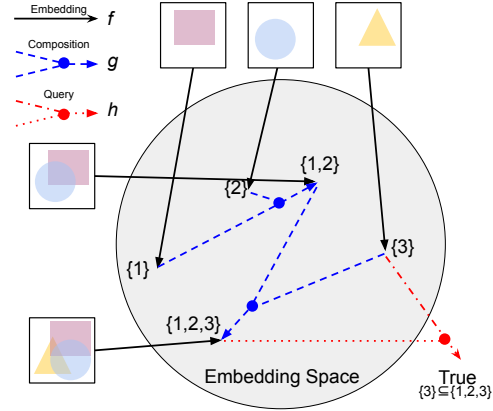


Figure 1. Overview of the paper: embedding function  $f$  is trained jointly with either a composition function  $g$  or a query function  $h$ . In particular, the goal is for  $g$  to “compose” the embeddings of two examples, containing classes  $\mathcal{T}$  and  $\mathcal{U}$  respectively, to approximate the embedding of an example containing classes  $\mathcal{T} \cup \mathcal{U}$ .

the dimensionality of the embedding space.

Previous research on embeddings has focused on cases where each example is associated with just one class (e.g., the image contains only one person’s face). In contrast, we investigate the case where each example is associated with not just one, but an *subset* of classes from a universe  $\mathcal{S}$ . The goal is to embed each example so that questions of two types can be answered (see Figure ??): (1) Is the set of classes in example  $x_a$  equal to the *union* of the classes in examples  $x_b$  and  $x_c$ ? (2) Does the set of classes in example  $x_a$  *subsume* the set of classes in example  $x_b$ ? For both these questions, we focus on settings in which the classes present in the example must be perceived automatically.

We approach this problem using *compositional set embeddings*. Like traditional embeddings, we train a function  $f$  that maps each example  $x \in \mathbb{R}^n$  into an embedding space  $\mathbb{R}^m$  so that examples with the same classes are mapped close together and examples with different classes are mapped far apart. Unlike traditional embeddings, our function  $f$  is trained to represent the *set* of classes that is associated with each example, so that questions about set union and subsumption can be answered by comparing vectors in the embedding space. We do not assume

<sup>1</sup>Department of Computer Science, Worcester Polytechnic Institute, Worcester, Massachusetts, USA <sup>2</sup>Google Brain. Correspondence to: Zeqian Li <zli14@wpi.edu>.

that the mechanism by which examples (e.g., images, audio signals) are rendered from multiple classes is known. Rather, the rendering process must be learned from training data. We propose two models, whereby  $f$  is trained jointly with either a “composition” function  $g$  (Model I) that answers questions about set union, or a “query” function  $h$  (Model II) that answers question about subsumption (see Figure ??).

To our best knowledge, this computational problem is novel. We see at least two use-cases: (1) Speaker recognition and diarization (i.e., infer who is talking within an audio signal) with multiple simultaneous speakers: Given an audio signal containing speakers who were not part of the training set and who may be speaking simultaneously, and given one example of each person speaking in isolation (one-shot learning), infer which *set* of speakers is talking. (2) Multi-object recognition in images: Given just the embedding of an image  $x_a$ , answer whether  $x_a$  contains the object(s) in another image  $x_b$ . Storing just the embeddings but not the pixels could potentially be more space-efficient and provide a form of image compression. Because of the novelty of the problem, it was not obvious to what baselines we should compare. When evaluating our models, we sought to assess the unique contribution of the *compositional* embedding above and beyond what traditional embedding methods achieve. Hence, we created baselines by endowing a traditional embedding with some extra functionality to enable it to infer label sets.

**Contribution:** To our knowledge, this is the first paper to explore how embedding functions can be trained both to *perceive* multiple objects in the example and to *represent* the set of detected objects so that set operations can be conducted among embedded vectors. We instantiate this idea in two ways: Model I for set union ( $f \& g$ ) and Model II for set containment ( $f \& h$ ). By evaluating on OmniGlott handwritten image data (Lake et al., 2015), LibriSpeech audio dataset (Panayotov et al., 2015), and the Open Images dataset (Kuznetsova et al., 2018), we provide a proof-of-concept that compositional set embeddings can work in one-shot learning scenarios. We also present evidence on COCO (Lin et al., 2014) that compositional embeddings can yield higher accuracy in standard supervised (not one-shot) learning settings for multi-label object recognition.

## 2. Related Work

**Embeddings:** We distinguish between two types of embeddings: (1) “Perceptual” embeddings such as for vision (Facenet Schroff et al., 2015) and speech (x-vector Snyder et al., 2018) where each class (e.g., person whose voice was recorded or face was photographed) may contain widely varying examples across speech content, facial expression, lighting, background noise, etc. (2) Word embed-

dings (word2vec (Mikolov et al., 2013), GloVe (Pennington et al., 2014)) where each class contains only one exemplar by definition. Within the former, the task of the embedding function is to map examples from the same class close together and examples from other classes far apart. This often requires deep, non-linear transformations to be successful. With word embeddings, the class of each example is already clear and does not need to be inferred; instead, the goal is to give the embedded vectors geometric structure to reflect co-occurrence, similarity in meaning, etc.

**Compositional embeddings:** Since at least 30 years, AI researchers, cognitive scientists, and computational neuroscientists have explored how the embeddings of multiple elements could be combined to reflect relationships between them or higher-level semantics. However, almost all this work was based on word embeddings, in which perception was not necessary. Some early work investigated how the grammatical structure and/or semantics of an input sentence can be represented (Pollack, 1989) in an efficient manner in neural networks, and how such a network could be trained (Elman, 1993). Given the advent of word embeddings, deep NLP architectures can combine the word-level semantics, as represented by the embeddings of the individual elements of an input sentence, to infer higher-level attributes, e.g., sentiment (Nakov et al., 2016). Recent work has investigated to what extent recurrent neural networks can generalize to understand novel sentences (Lake & Baroni, 2017) consisting of known words. Also, in the NLP domain, Joshi et al. (2018) developed compositional pairwise embeddings that model co-occurrence relationships between two words given their common context.

Probably the most algorithmically similar work to ours is by Lyu et al. (2019) on compositional network embeddings: the goal is to predict whether two new nodes in a graph, which were not observed during training, are adjacent, using node-based features as predictors. In their approach, two embeddings are used: one to embed the node-based features, and another to aggregate these embedded features into a secondary embedding space. Structurally, their work differs from ours in that (1) the two embedding spaces in their model do not represent the same universe of objects; (2) the embeddings do not capture set relationships.

**Deep set representations:** Our paper is also about how to encode a set of objects with a neural network. One issue is how to ensure invariance to the order in which examples are presented. Vinyals et al. (2015) proposed an approach based on permutation-invariant content-based attention. For producing sets as outputs, Rezatofighi et al. (2017) proposed a probabilistic model, within a supervised learning paradigm where all classes are known at training time, that predicts both the cardinality and the particular elements of the set.

### 3. Model I: Embedding $f$ and Composition $g$

**Assumptions and notation:** For generality, we refer to the data to be embedded (images, videos, audio signals, etc.) simply as “examples”. Let the universe of classes be  $\mathcal{S}$ . From any subset  $\mathcal{T} \subseteq \mathcal{S}$ , a ground-truth rendering function  $r : 2^{\mathcal{S}} \rightarrow \mathbb{R}^n$  “renders” an example, i.e.,  $r(\mathcal{T}) = x$ . Inversely, there is also a ground-truth classification function  $c : \mathbb{R}^n \rightarrow 2^{\mathcal{S}}$  that identifies the label set from the rendered example, i.e.,  $c(x) = \mathcal{T}$ . Neither  $r$  nor  $c$  is observed. We let  $e_{\mathcal{T}}$  represent the embedding (i.e., output of  $f$ ) associated with some example containing classes  $\mathcal{T}$ .

**Model:** Given two examples  $x_a$  and  $x_b$  that are associated with singleton sets  $\{s\}$  and  $\{t\}$ , respectively, the hope is that, for some third example  $x_c$  that is associated with *both* classes (i.e.,  $\{s, t\}$ ), we have

$$g(f(x_a), f(x_b)) \approx f(x_c)$$

Moreover, we hope that  $g$  can generalize to *any* number of classes within the set  $\mathcal{S}$ . For example, if example  $x_d$  is associated with a singleton set  $\{u\}$  and  $x_e$  is an example associated with  $\{s, t, u\}$ , then we hope

$$g(g(f(x_a), f(x_b)), f(x_d)) \approx f(x_e)$$

There are two challenging tasks that  $f$  and  $g$  must solve cooperatively: (1)  $f$  has to learn to perceive multiple objects that appear simultaneously and may possibly interact with each other – all *without* knowing the rendering process  $r$  of how examples are formed or how classes are combined. (2)  $g$  has to define geometrical structure in the embedding space to support set union operations. One way to understand our computational problem is the following: If  $f$  is invertible, then ideally we would want  $g$  to compute  $g(e_{\mathcal{T}}, e_{\mathcal{U}}) = f(r(c(f^{-1}(e_{\mathcal{T}})) \cup c(f^{-1}(e_{\mathcal{U}}))))$ . In other words, one (though not necessarily the only) way that  $g$  can perform well is to learn to perform the following actions (without knowing  $r$  or  $c$ ): (1) invert each of the two input embeddings; (2) classify the two corresponding label sets; (3) render an example with the union of the two inferred label sets; and (4) embed the result. Training  $f$  and  $g$  jointly may also ensure systematicity of the embedding space such that any combination of objects can be embedded.

**One-shot learning:** Model I can be used for one-shot learning on a set of classes  $\mathcal{S}$  not seen during training in the following way: We obtain  $k$  labeled examples  $x_1, \dots, x_k$  from the user, where each  $\{s_i\} = c(x_i)$  is the singleton set formed from the  $i$ th element of  $\mathcal{S}$  and  $|\mathcal{S}| = k$ . We call these examples the *reference examples*, and they provide a relatively strong form of supervision (compared to Model II in Section 4). We then infer which set of classes is represented by a new example  $x'$  using the following procedure:

(1) Compute the embedding of  $x'$ , i.e.,  $f(x')$ . (2) Use  $f$  to compute the embedding of each singleton example  $x_i$ , i.e.,  $e_{\{i\}} = f(x_i)$ . (3) From  $e_{\{1\}}, \dots, e_{\{k\}}$ , estimate the embedding of *every* subset  $\mathcal{T} = \{s_1, \dots, s_l\} \subseteq \mathcal{S}$  according to the recurrence relation:

$$e_{\{s_1, \dots, s_l\}} = g(e_{\{s_1, \dots, s_{l-1}\}}, e_{\{s_l\}}) \quad (1)$$

Finally, (4) estimate the label of  $x'$  as

$$\arg \min_{\mathcal{T} \subseteq \mathcal{S}} |f(x') - e_{\mathcal{T}}|^2 \quad (2)$$

Although the number of subsets is potentially exponential in  $|\mathcal{S}|$ , in some settings (e.g., speaker diarization) the maximum number of classes present in the example may be small, and thus the iteration is tractable.

#### 3.1. Training Procedure

Functions  $f$  and  $g$  are trained jointly: For each example  $x$  associated with classes  $\mathcal{T}$ , we compute  $e_{\mathcal{T}}$  from the singleton reference examples according to Equation 1. (To decide the order in which we apply the recursion, we define an arbitrary ordering over the elements of  $\mathcal{S}$  and iterate accordingly.) We then compute a hinge loss:

$$|f(x) - e_{\mathcal{T}}| \leq |f(x) - e_{\mathcal{T}'}| - \epsilon$$

for every  $\mathcal{T}' \neq \mathcal{T} \subseteq \mathcal{S}$ , where  $\epsilon$  is a small positive real number. In practice, for each example  $x$ , we randomly pick one element of  $\mathcal{T}' \in 2^{\mathcal{S}}$  for comparison. See Appendix for details on the training strategy and training-validation-test partition we used in the experiment, along with a discussion of an alternative (but less effective) training procedure.

#### 3.2. Experiment 1: OmniGlot

We first evaluated our method on the OmniGlot dataset (Lake et al., 2015). OmniGlot contains handwritten characters from 50 different alphabets; in total it comprises 1623 symbols, each of which was drawn by 20 people and rendered as a 64×64 image. OmniGlot has been previously used in one-shot learning research (e.g., Rezende et al., 2016; Bertinetto et al., 2016). In our experiment, the model is provided with one reference image for each singleton test class (5 classes in total). Then,  $f$  and  $g$  are used to select the subset of classes that most closely match the embedding of each test example (Equation 2). The goal is to train  $f$  and  $g$  so that, on classes not seen during training, the exact set of classes contained in each test example can be inferred.

We assessed to what extent the proposed model can capture set union operations. To create each example with label set  $\mathcal{T}$ , the rendering function  $r$  randomly picks one of the 20 exemplars from each class  $s \in \mathcal{T}$  and then randomly shifts, scales, and rotates it. Then,  $r$  computes the pixel-wise minimum across all the constituent images (one for each element of  $\mathcal{T}$ ). Finally,  $r$  adds Gaussian noise. See Figure 2

and the Appendix. Due to the complexity of each character as well as the overlapping pen strokes in composite images, recognizing the class label sets is quite challenging, even for humans.

In this experiment, we let the total number of possible speakers in each episode be  $k = 5$ . We trained  $f \& g$  such that the maximum class label set size was 3 (i.e.,  $|\mathcal{T}| \leq 3$ ). There are 25 such (non-empty) sets in total (5 singletons,  $\binom{5}{2} = 10$  2-sets, and  $\binom{5}{3} = 10$  3-sets).

**Architecture:** For  $f$ , we used ResNet-18 (He et al., 2016) that was modified to have 1 input channel and a 32-dimensional output. For  $g$ , we tested several architectures of increasing complexity. First, we defined  $\text{Symm}(a, b; k) = W_1 a + W_1 b + W_2(a \odot b)$  to be a symmetric function (with parameter matrices  $W_1, W_2$ ) of its two examples  $a, b \in \mathbb{R}^n$  that produces a vector in  $\mathbb{R}^k$ . Using this function, we compared four different architectures for  $g$ :

- **Mean** ( $g_{\text{Mean}}$ ):  $\frac{(a+b)}{2} \rightarrow \text{L2Norm}$ .
- **Bi-linear** ( $g_{\text{Lin}}$ ):  $\text{Symm}(a, b; 32) \rightarrow \text{L2Norm}$ .
- **Bi-linear + FC** ( $g_{\text{Lin+FC}}$ ):  $\text{Symm}(a, b; 32) \rightarrow \text{BN} \rightarrow \text{ReLU} \rightarrow \text{FC}(32) \rightarrow \text{L2Norm}$ .
- **DNN** ( $g_{\text{DNN}}$ ):  $\text{Symm}(a, b; 32) \rightarrow \text{BN} \rightarrow \text{ReLU} \rightarrow \text{FC}(32) \rightarrow \text{BN} \rightarrow \text{ReLU} \rightarrow \text{FC}(32) \rightarrow \text{BN} \rightarrow \text{ReLU} \rightarrow \text{FC}(32) \rightarrow \text{L2Norm}$ .

Here, BN is batch normalization, and  $\text{FC}(n)$  is a fully-connected layer with  $n$  neurons. We note that  $g_{\text{Mean}}$  is similar to the implicit form of compositionality discovered in word embedding models (Mikolov et al., 2013), e.g., woman – man + king = queen.

**Training:** For each mini-batch, 5 classes are randomly chosen from the universe  $\mathcal{S}$  (where  $|\mathcal{S}| = 944$  in training set). Images from these classes are rendered using function  $r$  from either singleton, 2-set class label sets, or 3-set class label sets. In other words,  $1 \leq |\mathcal{T}| \leq 3$  for all examples. See Appendix for more details. **Testing:** Testing data are generated similar to training data, but none of the classes were seen during training. We optimize Equation 2 to estimate the label set for each test example.

**Baselines:** We compared to two baselines:

- **Most frequent (MF):** Always guess the most frequent element in the test set. Since all classes occurred equally frequently, this was equivalent to random guessing.
- **Traditional embedding  $f$  and average (TradEmb):** We trained a traditional (i.e., non-compositional) embedding  $f$  just on singletons using one-shot learning

(Koch et al., 2015). (Accuracy on singletons after training: 97.9% top-1 accuracy in classifying test examples over 5 classes.) The embedding of a composite image with label set  $\mathcal{T}$  is then estimated using the mean of the embeddings of each class in  $\mathcal{T}$ . In contrast to  $g_{\text{Mean}}$  above, the  $f$  in this baseline is trained by itself, without knowledge of how its embeddings will be composed.

**Assessment:** We assessed accuracy (%-correct) in 3 ways:

- Accuracy, over all test examples, of identifying  $\mathcal{T}$ .
- Accuracy, over test examples for which  $|\mathcal{T}| = l$  (where  $l \in \{1, 2, 3\}$ ), of identifying  $\mathcal{T}$ . **Note:** we did *not* give the models the benefit of knowing  $\mathcal{T}$  – each model predicted the class label set over *all*  $\mathcal{T} \subset \mathcal{S}$  such that  $|\mathcal{T}| \leq 3$ . This can reveal whether a model is more accurate on examples with fewer vs. more classes.
- Accuracy, over all examples, in determining just the *number* of classes in the set, i.e.,  $|\mathcal{T}|$ .

**Results:** As shown in Table 1, the MF baseline accuracy was just 4% for an exact (top-1) match, and 12% for top-3 match. Using the TradEmb approach, accuracy increased to 25.5% and 40.9%, respectively. All of the proposed  $f \& g$  models outperformed the TradEmb baseline, suggesting that training  $f$  jointly with a composition function is helpful. For all the  $f \& g$  approaches as well as the TradEmb baseline, model predictions were well above chance (MF) for all label set sizes, i.e., these approaches could all distinguish label sets with more than one element at least to some degree.

Overall, the  $g_{\text{Lin}}$ , which contains a symmetric bi-linear layer prior to  $L_2$ -normalization, did the best: 64.7% and 87.6% for top-1 and top-3 matches over all examples, respectively. This suggests that composition by averaging alone is not optimal for this task. However, adding even more layers (i.e.,  $g_{\text{Lin+FC}}, g_{\text{DNN}}$ ) did not help, especially when the size  $\mathcal{T}$  increases. It is conceivable that the more complex  $g$  functions overfit, and that with regularization or more training data the deeper models might still prevail.

The Appendix describe an additional experiment about training and testing when we restrict  $|\mathcal{T}| \leq 2$ .

### 3.3. Experiment 2: LibriSpeech

Our second application is to detect who is speaking in audio clips when *multiple* people may be speaking at the same time. As this is a one-shot learning setting, we do not train on the speakers in test examples; rather, the model receives just one instance of each speaker as a reference example. Though overlapping speech occurs frequently in natural settings (e.g., meetings), only very few prior works



Ref.					
	{1}	{2}	{3}	{4}	{5}
Test					
	{1}	{2}	{3}	{4}	{5}
	{1,2}	{1,3}	{1,4}	{1,5}	{2,3}
	{2,4}	{2,5}	{3,4}	{3,5}	{4,5}
	{1,2,3}	{1,2,4}	{1,2,5}	{1,3,4}	{1,3,5}
	{1,4,5}	{2,3,4}	{2,3,5}	{2,4,5}	{3,4,5}

Figure 2. One set of reference and test images from the OmniGlott dataset, used in Experiments 1 and 3. Below each image is its associated class label set  $\mathcal{T}$ .

Experiment 1 (OmniGlott): Train with $ \mathcal{T}  \leq 3$							
Label Set Identification							
		$f \& g$ Approaches				Baselines	
		$g_{DNN}$	$g_{Lin+FC}$	$g_{Lin}$	$g_{Mean}$	TradEmb	MF
All	Exact	50.6	56.7	<b>64.7</b>	52.8	25.5	4.0
	Top-3	76.5	81.7	<b>87.6</b>	80.0	40.9	12.0
1-sets	Exact	94.5	96.0	<b>97.0</b>	86.9	89.3	4.0
	Top-3	99.1	99.4	<b>99.6</b>	95.4	96.6	12.0
2-sets	Exact	51.2	54.6	<b>64.5</b>	49.7	15.4	4.0
	Top-3	82.9	83.0	<b>87.9</b>	81.4	37.7	12.0
3-sets	Exact	27.9	39.1	<b>48.9</b>	39.0	3.7	4.0
	Top-3	58.7	71.6	<b>81.1</b>	71.1	16.4	12.0
Set Size Determination							
All		81.7	87.4	<b>90.1</b>	71.4	44.9	36.0

Table 1. Experiment 1 (OmniGlott): Mean accuracy (% correct) in inferring the label set of each example exactly (top 1), within the top 3, and the size of each label set. Set Size Determination measures the ability to infer the set size. Models are trained and tested with maximum class set size of 3.

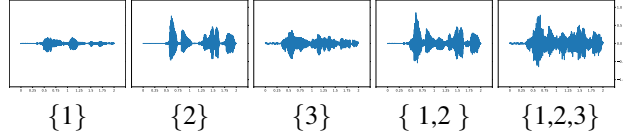


Figure 3. Examples of LibriSpeech audio waveforms from individual speakers and how they compose.

(e.g., Zelenak et al., 2012) have explored speaker diarization with multiple speakers.

In this experiment, LibriSpeech (Panayotov et al., 2015), which is a speech dataset based on LibriVox’s audio books, is used for training and evaluation. The training set, which consists of train-clean-100, train-clean-360 and train-other-500 subsets, has 2338 different speakers in total. The validation set, which is dev-clean, has 40 speakers. The test set, which consists of test-clean and test-other, has 73 speakers in total. Although LibriSpeech contains speech of only one person speaking at any time, we can generate samples with simultaneous speech from multiple speakers: The rendering function  $r$  randomly picks a 2-second recording clip for each speaker and sums the individual waveforms to a new mixture waveform (see Figure 3). It then extracts MFCC features (0.025s window size, 0.01s step size) from each waveform. Although the raw mixture of waveforms is linear, the MFCC feature representation of composite waveforms – which is a standard representation for speaker verification and diarization and what we use in our experiment – is non-linear in its constituent waveforms. Similar to Experiment 1, each data episode has 5 different speakers with at most 3 people speaking at once. Thus, there are 5 reference samples and 25 test samples. The Appendixs provide a URL to listen to some of the audio clips in our experiment (while preserving anonymity for review).

**Architecture:** For  $f$ , we use a 2-layer LSTM with 256 hidden units following by a 256-to-32 fully-connected layer. For  $g$ , we used the same functions  $g_{Mean}$ ,  $g_{Lin}$ ,  $g_{Lin+FC}$ , and  $g_{DNN}$ , as in Experiment 1.

**Baselines:** We use the same baselines as in Experiment 1, such that the TradEmb  $f$  function we trained achieves 95.3% top-1 accuracy over 5 singleton classes in one-shot fashion.

**Results:** As shown in Table 2, we observe the same trend as in Experiment 1. The proposed  $f \& g$  method easily outperforms the TradEmb and MF baselines, for all the different  $g$  we implemented. The baseline TradEmb performs relatively well on audio clips with single speakers (1-sets) but struggles on 2-sets or 3-sets. The slightly more powerful  $f \& g_{Mean}$  method (recall that the composition function has no trainable parameters) is more accurate than TradEmb, but the accuracy on 1-sets and for set size determination is

**Experiment 2 (LibriSpeech): Train with  $|\mathcal{T}| \leq 3$** 

Label Set Identification							
		$f \& g$ Approaches				Baselines	
		$g_{DNN}$	$g_{Lin+FC}$	$g_{Lin}$	$g_{Mean}$	TradEmb	MF
All	Exact	56.4	61.3	<b>72.1</b>	61.9	37.5	4.0
	Top-3	81.6	85.3	<b>91.7</b>	87.4	64.5	12.0
1-sets	Exact	91.2	92.4	<b>92.6</b>	79.6	77.6	4.0
	Top-3	98.1	<b>98.6</b>	98.5	92.0	90.6	12.0
2-sets	Exact	64.6	66.3	<b>75.9</b>	62.3	34.4	4.0
	Top-3	88.6	88.8	<b>93.7</b>	88.5	67.2	12.0
3-sets	Exact	30.8	40.7	<b>57.9</b>	52.6	20.6	4.0
	Top-3	66.4	75.2	<b>86.4</b>	84.0	48.7	12.0
Set Size Determination							
All		76.7	87.1	<b>92.5</b>	73.6	56.5	36.0

Table 2. **Experiment 2 (LibriSpeech):** Mean accuracy (% correct) in inferring the label set of each example exactly (top 1), within the top 3, and the size of each label set. Set Size Determination measures the ability to decide the correct set size. Models are trained and tested with maximum class set size of 3.

worse than the other  $g$  methods that have parameters. As in Experiment 1, the  $g_{Lin}$  usually performs the best. When we stack more FC layers, the performance gets worse, especially on audio clips associated with 3 classes.

**Discussion:** Experiments 1 and 2 suggest that, for  $f \& g$  compositionality for set union, a simple linear layer works best. One possible explanation is that  $g_{Lin}$ , despite the L2Norm at the end, might retain a greater degree of associativity (i.e.,  $(a + b) + c = a + (b + c)$ ) than deeper  $g$  functions. This property may be important especially for larger  $\mathcal{T}$ , where  $g$  is invoked multiple times to create larger and larger set unions.

#### 4. Model II: Embedding $f$ and Query $h$

In some applications, it may be more useful to determine whether an example *contains* an object or set of objects. For instance, we might want to know whether a speaker’s voice is part of a conversation, or whether a specific object is in an image. Moreover, in some settings, it may be difficult during training to label every example (video, audio clip, etc.) for the presence of *all* the objects it contains – for each example, we might only know its labels for a subset of classes. Here we propose a second type of compositional embedding mechanism that tests whether the set of classes associated with one example *subsumes* the set of classes associated with another example. We implement this using a “query” function  $h$  that takes two embedded examples as inputs:

$$h(f(x_a), f(x_b)) = \text{True} \iff c(x_b) \subseteq c(x_a) \quad (3)$$

**Experiment 3 (OmniGlott)**

	$h_{DNN}$	$h_{Lin+FC}$	$h_{Lin}$	TradEmb
% Correct	<b>71.8</b>	71.1	50.8	63.8
AUC	<b>80.0</b>	79.1	51.4	78.2

**Experiment 4 (LibriSpeech)**

	$h_{DNN}$	$h_{Lin+FC}$	$h_{Lin}$	TradEmb
% Correct	<b>77.5</b>	76.8	50.1	74.4
AUC	<b>86.3</b>	85.8	50.1	84.3

**Experiment 5 (Open Images)**

	$h_{DNN}$	$h_{Lin+FC}$	$h_{Lin}$	TradEmb
% Correct	<b>76.9</b>	76.8	50.0	50.1
AUC	<b>85.4</b>	85.2	50.3	59.2

Table 3. **Experiments 3, 4, and 5:** Accuracy to query whether the classes in one example subsume the classes in another example, for the proposed  $f \& h$  method versus a traditional embedding function  $f$  (TradEmb) as a baseline.

In contrast to  $g$ , function  $h$  is not symmetric: its first and second arguments are the putative superset and subset, respectively. Also,  $h$  can be trained with only relatively weak supervision w.r.t. the individual examples: it never needs to know which exact label set is associated with an example, but rather only *pairwise* information about which examples “subsume” other examples. In Experiments 3, 4, and 5, we evaluate our models in the setting of one-shot learning, i.e., the classes of test samples were never seen during training.

#### 4.1. Training procedure

Functions  $f$  and  $h$  are trained jointly. Since  $h$  is not symmetric, its first layer is replaced with a linear layer  $W_1 a + W_2 b$  (see Appendix). In contrast to Model I, “reference” examples are not needed; only the subset relationships between label sets of pairs of examples are required. To train  $f$  and  $h$ , we backpropagate a binary cross-entropy loss, based on correctly answering the query in Eq. 3, through  $h$  to  $f$ .

#### 4.2. Experiment 3: OmniGlott

Here we assess Model II on OmniGlott where size of class label sets is up to 5, and we use the same rendering function  $r$  in Experiment 2. Let  $f(x_a)$  and  $f(x_b)$  be the two arguments to  $h$ . For  $x_a$ , it can be associated with multiple classes, from 1 class (i.e.,  $c(x_a) = \{s_1\}$ ) to 5 classes (i.e.,  $c(x_a) = \{s_1, s_2, \dots, s_5\}$ ), where all label sets occur with equal frequency. For  $x_b$ , half are positive examples (i.e., such that  $h(f(x_a), f(x_b)) = \text{True}$ ) which are associated with classes contained in  $x_a$ , so that  $c(x_b) \subseteq c(x_a)$ . The other half are negative examples ( $h(f(x_a), f(x_b)) = \text{False}$ ), where  $x_b$  is associated with some other singleton class  $c(x_b) \not\subseteq c(x_a)$ . Both the training set and test set have

this configuration.

**Architecture:** For  $f$ , we used the same architecture as in Experiment 1. For  $h$ , we tried several functions ( $h_{\text{DNN}}$ ,  $h_{\text{Lin+FC}}$ ,  $h_{\text{Lin}}$ ), analogous to the different implementations of  $g$  from Section 3.2 except that the final layers have a 1-dimensional sigmoid output. See Appendix for more details.

**Baseline:** We compared our proposed method with a traditional (non-compositional) embedding method (**TradEmb**) that is trained to separate examples according to their association with just a *single* class. In particular, for each composite example  $x_a$  (i.e.,  $|c(x_a)| = 2$ ), we picked one of the two classes arbitrarily (according to some fixed ordering on the elements of  $\mathcal{S}$ ); call this class  $s_1$ . Then, we chose both a positive example  $x_b$  (such that  $c(x_b) = \{s_1\}$ ) and a negative example  $x_c$  (such that  $c(x_c) = \{s_3\} \not\subseteq c(x_a)$ ). We then compute a hinge loss so that the distance between  $f(x_a)$  and  $f(x_b)$  is smaller than the distance between  $f(x_a)$  and  $f(x_c)$ , and backpropagate the loss through  $f$ . During testing, we use  $f$  to answer a query—does  $c(x_a)$  contain  $c(x_b)$ ?—by thresholding the distance between  $f(x_a)$  and  $f(x_b)$  (threshold of 0.5).

**Results** are shown in Table 3 (top). Compositional embeddings, as implemented with a combination of  $f$  trained jointly with either  $h_{\text{DNN}}$  or  $h_{\text{Lin+FC}}$ , outperform the TradEmb baseline, in terms of both % correct accuracy and AUC. Unlike in Model I, where  $h_{\text{Lin}}$  achieved the best results,  $f$  trained jointly with  $h_{\text{Lin}}$  is just slightly better than random guess (50%). We observed an advantage of deeper architectures for  $h$ .

#### 4.3. Experiment 4: LibriSpeech

We also assessed Model II on LibriSpeech with up to 5 simultaneous speakers. The rendering function  $r$  is the same as in Experiment 2. Training and evaluation follow the same settings in Experiment 3. **Architectures:** We used the same ones as in Experiment 2, except the size of the output layer for  $h$  is 1. We also used a TradEmb baseline like in Experiment 3.

**Results** are in Table 3 (middle). We observe the same conclusion as in Experiment 3: The compositional embedding model substantially outperforms the TradEmb baseline, and the deeper  $h$  (i.e.,  $h_{\text{DNN}}$ ,  $h_{\text{Lin+FC}}$ ) perform best.

#### 4.4. Experiment 5: Open Images

Here we trained and evaluated Model II on Open Images (Kuznetsova et al., 2018). This dataset contains a total of 16M bounding boxes for 600 object classes on 1.9M images. This is a highly challenging problem: in the example in Figure 4,  $f$  has to encode a dog, trousers and footwear; then, given completely different images of these classes

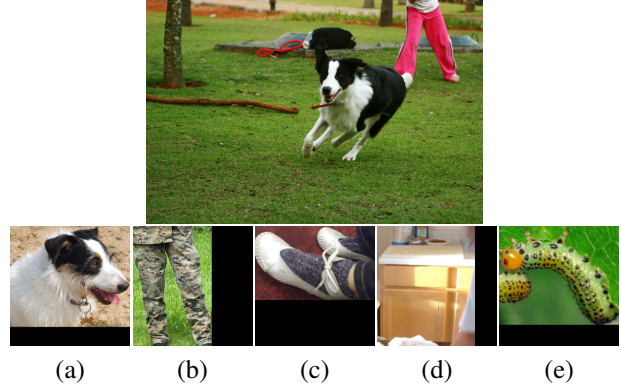


Figure 4. **Experiment 5 (Open Images):** An example image (top) of a running dog and the lower body of a human. The image is padded to form a square and downsampled. The composite embedding with  $f$  is computed and then queried with  $h$  about the presence of the object in images (a-e), containing *dog*, *trousers*, *footwear*, *countertop*, and *caterpillar*. The query function  $h$ , when given the embeddings of the top image and another image, should return True for (a,b,c) and False for (d,e).

(and others),  $h$  has to decide which objects were present in the original image. In Open Images, each image may contain objects from multiple classes, and each object has a bounding box. We acquire singleton samples by using the bounding boxes to crop singleton objects from images. In this experiment, 500 classes are selected for training and 73 other classes for testing. The training and evaluation settings are the same as Experiment 3. We also use a TradEmb baseline like in Experiment 3. **Architectures:** For  $f$ , we use ResNet-18 that was modified to have a 32-dimensional output. We used the same  $h$  as in Experiment 3.

**Results** are shown in Table 3 (bottom). The compositional embedding models consisting of  $f$  combined with either  $h_{\text{DNN}}$  and  $h_{\text{Lin+FC}}$  easily outperformed the TradEmb baseline. However, with  $h_{\text{Lin}}$  the accuracy is not much better than chance. It is likely that the traditional embedding approach is not able to capture containment relationships in such a challenging dataset.

**Discussion:** One interesting phenomenon we discovered is that while the linear model  $g_{\text{Lin}}$  achieves the best results in the  $f \& g$  setting (set union), it is hardly better than random chance for the  $f \& h$  setting (set containment). On the other hand, while  $g_{\text{DNN}}$  is worse than other trainable  $g$  functions for set union, it outperforms the other functions for set containment. We do not have a complete explanation for this finding. One possibility is that training  $f$  in Model I to distinguish explicitly between all possible subsets causes  $f$  to become very powerful (relative to the  $f$  trained in Model II), after which only a simple  $g$  is required to compute set unions. The training procedure in Model II based on set containment might provide less information to  $f$ , thus re-

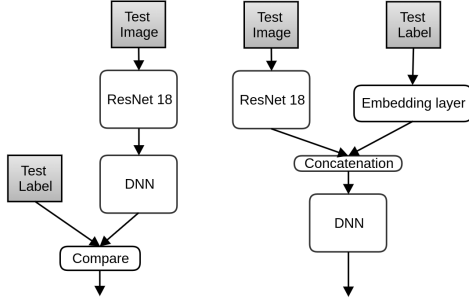


Figure 5. **Experiment 6 (COCO)**: Left shows baseline. Right shows proposed  $f \& h$  method.

quiring  $g$  to be more powerful to compensate. Another possibility is that, since  $g$  may be applied several times recursively to construct larger and larger unions, its complexity must be kept small to avoid overfitting.

#### 4.5. Experiment 6: COCO

Given the promising results on one-shot learning tasks for object recognition, we performed one final experiment to assess whether compositional embeddings could be beneficial for multi-label classification in standard supervised learning problems where the testing and training classes are the same (i.e., *not* one-shot). Specifically, we seek to develop a model to answer questions of the form, “Does image  $x$  contain an object of class  $y$ ?”. One approach to this task is to train a CNN (e.g., ResNet) with multiple independent sigmoid outputs (one for each class), and then to check whether the output for the desired label is close to 1. We compare this baseline to the following compositional embedding method that uses *three* functions trained jointly: (1) A deep embedding  $f_{\text{im}}$  for the input image; (2) A linear layer  $f_{\text{label}}$  to embed a one-hot vector of the queried label into a distributed representation; and (3) a query function  $h$  that takes the two embeddings as inputs and outputs the probability that the image contains an object with the desired label. In contrast to the ResNet baseline, this approach enables the combined network to modulate its perception of the objects contained within an image based on the specific task, i.e., the specific label that was queried, which may help it to perform more accurately (Mozer & Fan, 2008). We conducted our comparison of these approaches on the COCO (Lin et al., 2014) dataset, which has  $|\mathcal{S}| = 80$  classes in both the training and validation sets. During evaluation, half the test labels are positive and the other half are negative. See Appendixs.

**Baseline:** See Figure 5 (left). The dimension of ResNet-18’s last layer is modified to 128. The DNN consists of  $\text{FC}(128) \rightarrow \text{BN} \rightarrow \text{ReLU} \rightarrow \text{FC}(128) \rightarrow \text{BN} \rightarrow \text{ReLU} \rightarrow \text{FC}(128) \rightarrow \text{Sigmoid}(80)$ , where  $\text{Sigmoid}(k)$

is a sigmoidal layer with  $k$  independent probabilistic outputs. Log loss over all classes are summed up for each image during backpropagation. Because of class imbalance, different weights are used for positive and negative classes according to their numbers in each image.

**Architecture:** See Figure 5 (right). The dimension of ResNet-18’s last layer is modified to 128. The embedding layer maps 80-class labels to 32-dimension embeddings. Then the image embedding and label embedding are concatenated to a 160-dimension vector. The DNN consists by  $\text{FC}(160) \rightarrow \text{BN} \rightarrow \text{ReLU} \rightarrow \text{FC}(136) \rightarrow \text{BN} \rightarrow \text{ReLU} \rightarrow \text{FC}(136) \rightarrow \text{Sigmoid}(1)$ . Binary cross entropy is used as the loss function. This architecture uses the same ResNet for image embedding extraction as the baseline, and the DNN has almost the same number of parameters.

**Results:** The baseline accuracy using the ResNet attained an accuracy of 64.0% and AUC is 67.7%. In contrast, the compositional embedding approach ( $f_{\text{im}} \& f_{\text{label}} \& h$ ) achieved a substantially higher accuracy of 82.0% and AUC is 90.8%. This accuracy improvement may stem from the task modulation of the visual processing (Mozer & Fan, 2008), or from the fact that the compositional method was explicitly designed to answer binary image queries rather than represent the image as a  $|\mathcal{S}|$ -dimensional vector (as with a standard object recognition CNN).

## 5. Conclusions

We proposed a new kind of embedding mechanism whereby the *set* of objects contained in the input data (e.g., image, audio) must be both *perceived* and then mapped into a space such that the *set relationships* – union (Model I) and containment (Model II) – between multiple embedded vectors can be inferred. Importantly, the ground-truth rendering process for how examples are rendered from their component classes is not known and must implicitly be learned. In our experiments, conducted on OmniGlot, LibriSpeech and Open Images, the accuracy was far from perfect but outperformed the baseline based on a traditional embedding approach. The results provide a proof-of-concept of how an embedding function  $f$ , trained jointly with either the composition function  $g$  or the query function  $h$ , could be effectively optimized. One possible direction for further research – motivated by perceptual expertise research on, for example, how chess experts perceive real versus random game configurations (Chase & Simon, 1973) – is to take better advantage of the statistical structure of class co-occurrence in a specific application domain (e.g., which objects tend to co-occur in the same image).



## References

- Bertinetto, L., Henriques, J. F., Valmadre, J., Torr, P., and Vedaldi, A. Learning feed-forward one-shot learners. In *Advances in Neural Information Processing Systems*, pp. 523–531, 2016.
- Chase, W. G. and Simon, H. A. Perception in chess. *Cognitive psychology*, 4(1):55–81, 1973.
- Elman, J. L. Learning and development in neural networks: The importance of starting small. *Cognition*, 48(1):71–99, 1993.
- He, K., Zhang, X., Ren, S., and Sun, J. Deep residual learning for image recognition. In *Proceedings of the IEEE conference on computer vision and pattern recognition*, pp. 770–778, 2016.
- Joshi, M., Choi, E., Levy, O., Weld, D. S., and Zettlemoyer, L. pair2vec: Compositional word-pair embeddings for cross-sentence inference. *arXiv preprint arXiv:1810.08854*, 2018.
- Koch, G., Zemel, R., and Salakhutdinov, R. Siamese neural networks for one-shot image recognition. In *ICML deep learning workshop*, volume 2, 2015.
- Kuznetsova, A., Rom, H., Alldrin, N., Uijlings, J., Krasin, I., Pont-Tuset, J., Kamali, S., Popov, S., Mallocci, M., Duerig, T., and Ferrari, V. The open images dataset v4: Unified image classification, object detection, and visual relationship detection at scale. *arXiv:1811.00982*, 2018.
- Lake, B. M. and Baroni, M. Generalization without systematicity: On the compositional skills of sequence-to-sequence recurrent networks. *arXiv preprint arXiv:1711.00350*, 2017.
- Lake, B. M., Salakhutdinov, R., and Tenenbaum, J. B. Human-level concept learning through probabilistic program induction. *Science*, 350(6266):1332–1338, 2015.
- Lin, T.-Y., Maire, M., Belongie, S., Hays, J., Perona, P., Ramanan, D., Dollár, P., and Zitnick, C. L. Microsoft coco: Common objects in context. In *European conference on computer vision*, pp. 740–755. Springer, 2014.
- Lyu, T., Sun, F., Jiang, P., Ou, W., and Zhang, Y. Compositional network embedding for link prediction. In *Proceedings of the 13th ACM Conference on Recommender Systems*, pp. 388–392, 2019.
- Mikolov, T., Chen, K., Corrado, G., and Dean, J. Efficient estimation of word representations in vector space. *arXiv preprint arXiv:1301.3781*, 2013.
- Mozer, M. C. and Fan, A. Top-down modulation of neural responses in visual perception: a computational exploration. *Natural Computing*, 7(1):45–55, 2008.
- Nakov, P., Ritter, A., Rosenthal, S., Sebastiani, F., and Stoyanov, V. Semeval-2016 task 4: Sentiment analysis in twitter. In *Proceedings of the 10th international workshop on semantic evaluation (semeval-2016)*, pp. 1–18, 2016.
- Panayotov, V., Chen, G., Povey, D., and Khudanpur, S. Librispeech: an asr corpus based on public domain audio books. In *2015 IEEE International Conference on Acoustics, Speech and Signal Processing (ICASSP)*, pp. 5206–5210. IEEE, 2015.
- Pennington, J., Socher, R., and Manning, C. Glove: Global vectors for word representation. In *Proceedings of the 2014 conference on empirical methods in natural language processing (EMNLP)*, pp. 1532–1543, 2014.
- Pollack, J. B. Implications of recursive distributed representations. In *Advances in neural information processing systems*, pp. 527–536, 1989.
- Rezatofighi, S. H., Milan, A., Abbasnejad, E., Dick, A., Reid, I., et al. Deepsetnet: Predicting sets with deep neural networks. In *2017 IEEE International Conference on Computer Vision (ICCV)*, pp. 5257–5266. IEEE, 2017.
- Rezende, D. J., Mohamed, S., Danihelka, I., Gregor, K., and Wierstra, D. One-shot generalization in deep generative models. *arXiv preprint arXiv:1603.05106*, 2016.
- Schroff, F., Kalenichenko, D., and Philbin, J. Facenet: A unified embedding for face recognition and clustering. In *Proceedings of the IEEE conference on computer vision and pattern recognition*, pp. 815–823, 2015.
- Scott, T., Ridgeway, K., and Mozer, M. C. Adapted deep embeddings: A synthesis of methods for k-shot inductive transfer learning. In *Advances in Neural Information Processing Systems*, pp. 76–85, 2018.
- Sell, G., Snyder, D., McCree, A., Garcia-Romero, D., Villalba, J., Maciejewski, M., Manohar, V., Dehak, N., Povey, D., Watanabe, S., et al. Diarization is hard: Some experiences and lessons learned for the jhu team in the inaugural dihard challenge. In *Interspeech*, pp. 2808–2812, 2018.
- Snyder, D., Garcia-Romero, D., Sell, G., Povey, D., and Khudanpur, S. X-vectors: Robust dnn embeddings for speaker recognition. In *2018 IEEE International Conference on Acoustics, Speech and Signal Processing (ICASSP)*, pp. 5329–5333. IEEE, 2018.
- Vinyals, O., Bengio, S., and Kudlur, M. Order matters: Sequence to sequence for sets. *arXiv preprint arXiv:1511.06391*, 2015.

Zelenak, M., Segura, C., Luque, J., and Hernando, J. Simultaneous speech detection with spatial features for speaker diarization. *IEEE Transactions on Audio, Speech, and Language Processing*, 20(2):436–446, 2012.

## A. Alternative Training Procedure

We also tried another method of training  $f$  and  $g$  with the explicit goal of encouraging  $g$  to map  $e_{\mathcal{T}}$  and  $e_{\mathcal{U}}$  to be close to  $e_{\mathcal{T} \cup \mathcal{U}}$ . This can be done by training  $f$  and  $g$  alternately, or by training them jointly in the same backpropagation. However, this approach yielded very poor results. A possible explanation is that  $g$  could fulfill its goal by mapping all vectors to the same location (e.g.,  $\mathbf{0}$ ). Hence, a trade-off arises between  $g$ 's goal and  $f$ 's goal (separating examples with distinct label sets).

## B. Details of Experiment 1: OmniGlot

There are 944 characters in training set, 20 characters in validation set, 659 characters in test set.

To generate a data episode, the rendering function  $r$  (1) randomly picks 5 character classes; (2) for each character class randomly selects one image as reference image and one as test image; (3) for each image from previous step applies random affine transformations consisting of shift up to 20%, scaling up to 10%, and rotation up to  $10^\circ$ ; (4) generates all possible combinations of 2-sets and 3-sets by taking the minimum value of multiple test images; (5) adds Gaussian noise with mean 0.9 and variance 0.1.

We generate 100,000 episodes for training set, 1,000 episodes for validation set and 10,000 episodes for test set.

Training is performed using Adam ( $\text{lr} = .0003$ ) to maximize the validation accuracy. Every mini-batch contains one data episode. We set the hinge parameter  $\epsilon = 0.1$  when computing loss. We do not explore other hyperparameters as our focus is to make comparison of different architectures. The model is trained and evaluated once.

We also conduct another experiment with  $|\mathcal{T}| \leq 2$ , while other settings are the same. Results can be found in Figure 4.

## C. Details of Experiment 2: LibriSpeech

There are 2,338 speakers in training set, 40 speakers in validation set, 73 speakers in test set.

To generate a data episode, the rendering function  $r$  (1) randomly picks 5 speakers; (2) for each speaker random selects one 2-second recording clip as reference sample and one as test sample; (3) generates all possible combinations

### Experiment 1 (OmniGlot): Train with $|\mathcal{T}| \leq 2$

		Label Set Identification					
		$f \& g$ Approaches				Baselines	
		$g_{\text{DNN}}$	$g_{\text{Lin+FC}}$	$g_{\text{Lin}}$	$g_{\text{Mean}}$	Mean	MF
All	Exact	77.8	77.7	81.5	75.3	43.7	6.7
	Top-3	95.4	95.1	96.8	93.8	67.6	20.0
1-sets	Exact	97.4	95.8	96.7	88.0	89.8	6.7
	Top-3	99.5	99.1	99.4	98.3	98.9	20.0
2-sets	Exact	68.0	68.6	73.9	68.9	20.6	6.7
	Top-3	93.3	93.1	95.4	91.5	51.9	20.0
		Set Size Determination					
All		96.5	96.6	97.2	90.5	76.7	55.6

Table 4. **Experiment 1 (OmniGlot with  $|\mathcal{T}| \leq 2$ ):** Mean accuracy (% correct) in inferring the label set of each example exactly (top 1), within the top 3, and the size of each label set. Set Size Determination measures the ability to infer the set size. Models are trained and tested with maximum class set size of 2.

of 2-sets and 3-sets by computing the sum of multiple test samples; (4) extracts MFCC features from all test samples and reference samples using 0.025-second window size, 0.01-second step size and 32 cepstrum coefficients.

(Some example clips can be find in this URL <https://drive.google.com/open?id=1L3rNK1FXcjN5Toc5dq-BzwV-3hnAYiaV>.)

We generate 100,000 episodes for training set, 1,000 episodes for validation set and 10,000 episodes for test set.

Training is performed using Adam ( $\text{lr} = .0003$ ) to maximize the validation accuracy. Every mini-batch contains 32 data episode. We set the hinge parameter  $\epsilon = 0.1$  when computing loss. These are the only hyperparameters explored. The model is trained and evaluated once.

We also conduct another experiment with  $|\mathcal{T}| \leq 2$ , while other settings are the same. Results can be found in Figure 5.

## D. Details of Experiment 3: OmniGlot

Same as Experiment 1, there are 944 characters in training set, 20 characters in validation set, 659 characters in test set.

To generate a data episode, the rendering function  $r$  (1) randomly picks  $\mathcal{T}$  character classes ( $2 \leq \mathcal{T} \leq 6$ ); (2) for the 1st character class randomly picks one image as positive sample; for each character classes from 1st to  $(\mathcal{T} - 1)th$  randomly picks one image as singleton candidate; for the  $\mathcal{T}th$  character class randomly picks one image as negative sample; (3) for each image from previous step applies random affine transformations consisting of shift up to 20%,

**Experiment 2 (LibriSpeech): Train with  $|\mathcal{T}| \leq 2$** 

Label Set Identification							
		$f \& g$ Approaches				Baselines	
		$g_{DNN}$	$g_{Lin+FC}$	$g_{Lin}$	$g_{Mean}$	Mean	MF
All	Exact	82.2	84.5	84.9	78.9	61.1	6.7
	Top-3	96.2	97.4	97.6	95.8	88.1	20.0
1-sets	Exact	92.1	93.8	94.0	79.5	78.9	6.7
	Top-3	97.1	98.4	98.6	95.6	95.8	20.0
2-sets	Exact	77.3	79.9	80.4	78.5	52.2	6.7
	Top-3	95.7	96.9	97.2	95.8	84.2	20.0
Set Size Determination							
All		99.2	99.2	99.1	90.3	80.0	55.6

Table 5. **Experiment 2 (LibriSpeech):** Mean accuracy (% correct) in inferring the label set of each example exactly (top 1), within the top 3, and the size of each label set. Set Size Determination measures the ability to decide the correct set size. Models are trained and tested with maximum class set size of 2.

scaling up to 10%, and rotation up to  $10^\circ$ ; (4) generates the compositional image by taking the minimum value of the singleton candidates; (5) adds Gaussian noise with mean 0.9 and variance 0.1.

We generate 100,000 episodes for training set, 1,000 episodes for validation set and 10,000 episodes for test set.

Unlike Experiment 1, the symmetric function of  $h$ 's first layer is replaced by (1)  $W_1 a + W_2 b$  in  $g_{Lin}$ ,  $g_{Lin+FC}$  and  $g_{DNN}$ ; (2)  $WCat(a, b)$  in  $g_{Mean}$ , where  $Cat(a, b)$  is concatenation of  $a$  and  $b$ . The output dimension of each  $h$ 's last layer is modified to 1.

Training is performed using Adam ( $lr = .0003$ ) to maximize the validation accuracy. Every mini-batch contains 128 data episode. Binary cross entropy is used as loss function. The model is trained and evaluated once.

Additionally, we also plot the relationship between accuracy/AUC and number of singletons in compositional sample ( $\mathcal{T}$ ). See in Figure 6.

## E. Details of Experiment 4: LibriSpeech

Same as Experiment 2, there are 2,338 speakers in training set, 40 speakers in validation set, 73 speakers in test set.

To generate a data episode, the rendering function  $r$  (1) randomly picks  $\mathcal{T}$  speakers ( $2 \leq \mathcal{T} \leq 6$ ); (2) for the 1st speaker randomly picks one 2-second clip as positive sample; for each speaker from 1st to  $(\mathcal{T} - 1)th$  randomly picks one sample as singleton candidate; for the  $\mathcal{T}th$  speaker randomly picks one clip as negative sample; (3) generates the compositional sample by computing the sum of all singleton candidates; (4) extracts MFCC features from all sam-

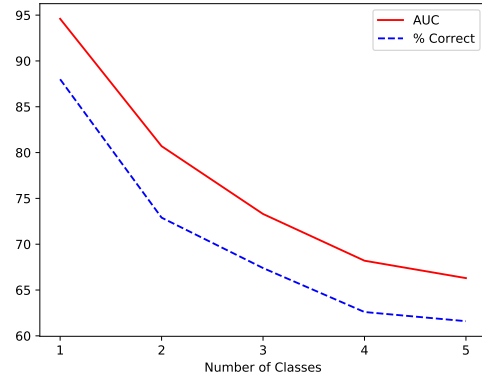


Figure 6. In OmniGlot,  $h_{DNN}$ 's results according to the number of subclasses contained in images

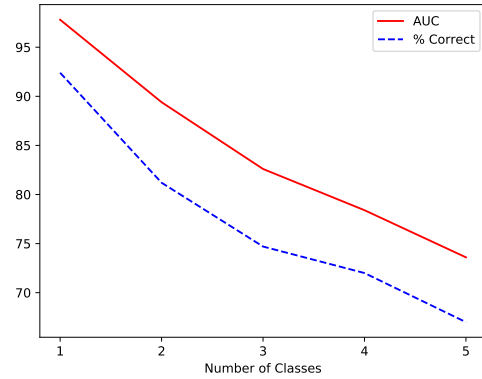


Figure 7. In LibriSpeech,  $h_{DNN}$ 's results according to the number of subclasses contained in images

ples.

We generate 100,000 episodes for training set, 1,000 episodes for validation set and 10,000 episodes for test set.

In this experiment, function  $h$  is the same as Experiment 3.

Training is performed using Adam ( $lr = .0003$ ) to maximize the validation accuracy. Every mini-batch contains 128 data episode. Binary cross entropy is used as loss function. The model is trained and evaluated once.

Additionally, we also plot the relationship between accuracy/AUC and number of singletons in compositional sample ( $\mathcal{T}$ ). See in Figure 7.

## F. Details of Experiment 5: Open Images

In Open Images, there are 1,743,042 training images, 41,620 validation images and 125,436 test images. There

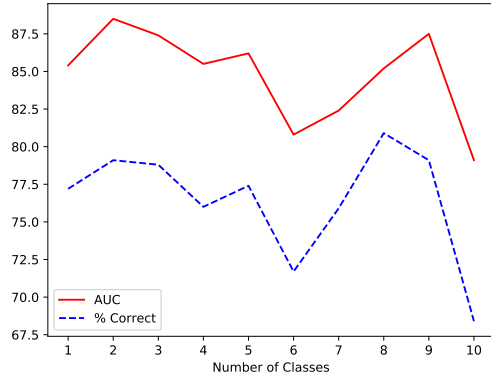


Figure 8. In Open Images,  $h_{DNN}$ 's results according to the number of subclasses contained in images: Results of images contain more than 10 labeled objects are not show because they are too few in test set.

are 600 classes of objects contained in these images in total. In order to make sure that object classes in evaluation are not seen during training, 500 classes are used for training (validation set also uses the same 500 classes) and 73 classes are used for testing (Not all 600 classes are included in test set).

All objects are cropped according to their bounding boxes, and then resized and padded to  $256 \times 256$ . All original images are also resized and padded to the same size.

We also generate two mapping dictionaries: (1) images and the classes of the objects they contained; (2) object classes and all images that contain them.

To generate a data episode, we (1) randomly pick one class as positive class; (2) randomly pick one test image that contains the positive class; (3) randomly pick one negative class that is not contained in the test image; (4) randomly pick one object image from positive class and one from negative class.

We generate 100,000 episodes for training set, 1,000 episodes for validation set and 10,000 episodes for test set.

In this experiment, function  $h$  is the same as Experiment 3.  $f$  is ResNet pretrained on ImageNet.

Training is performed using Adam ( $lr = 3 \times 10^{-8}$  for  $f$ ,  $lr = 3 \times 10^{-8}$  for  $h$ ) to maximize the validation accuracy. Every mini-batch contains 32 data episode. Binary cross entropy is used as loss function. The model is trained and evaluated once.

Additionally, we also plot the relationship between accuracy/AUC and number of singletons in compositional sample ( $\mathcal{T}$ ). See in Figure 8

## G. Details of Experiment 6: COCO

In this experiment, there are 118,287 images in training set, 5,000 images in validation set, 40670 images in test set. All images contain 80 classes of objects in total.

We use the same method as Experiment 5 to generate data episodes. 100,000 episodes are generated for training set, 1,000 episodes for validation set and 10,000 episodes for test set.

In this experiment, function  $h$  is the same as Experiment 3.  $f$  is ResNet pretrained on ImageNet.

Training is performed using Adam ( $lr = 3 \times 10^{-8}$  for  $f$ ,  $lr = 3 \times 10^{-8}$  for  $h$ ) to maximize the validation accuracy. Every mini-batch contains 32 data episode. Binary cross entropy is used as loss function. The model is trained and evaluated once.

All experiments are conducted on one NVIDIA TITAN RTX and one NVIDIA GEFORCE GTX 1080 Ti.